JBC RESEARCH ARTICLE

Titin cleavage in living cardiomyocytes induces sarcomere disassembly but does not trigger cell proliferation

Received for publication, November 3, 2025, and in revised form, May 4, 2026 Published, Papers in Press, May 15, 2026
https://doi.org/10.1016/j.jbc.2026.113167

Maria Rosaria Pricolo[1,*], Miguel A. López-Unzu[1], Natalia Vicente[1], Cristina Morales-López[1], Carla Huerta-López[1], Wendy Pérez-Franco[1], Andra C. Dumitru[1,2], Jorge Peña-Peña[1], Francisco M. Espinosa[3], Mateo I. Sanchez[4], Ricardo Garcia[3], Roberto Silva-Rojas[1], Miguel Torres[1,5], Elías Herrero-Galán[1], and Jorge Alegre-Cebollada[1,5,*]

From the [1]Centro Nacional de Investigaciones Cardiovasculares (CNIC), Madrid, Spain; [2]Louvain Institute of Biomolecular Science and Technology, Universite catholique de Louvain, Louvain-la-Neuve, Belgium; [3]Instituto de Ciencia de Materiales de Madrid (ICMM), Madrid, Spain; [4]Yusuf Hamied Department of Chemistry, University of Cambridge, Cambridge, United Kingdom; [5]Centro de Investigación Biomédica en Red de Enfermedades Cardiovasculares (CIBERCV), Madrid, Spain

Reviewed by members of the JBC Editorial Board. Edited by Enrique De La Cruz

Adult mammalian hearts have limited regenerative capacity due to the inability of cardiomyocytes to proliferate, a major clinical hurdle in contemporary cardiology. The presence of highly organized, contractile sarcomeres has long been considered an impediment for cardiomyocyte division. Indeed, sarcomere disassembly is a crucial step to complete the cell cycle in the few situations where cardiomyocytes have been observed to proliferate. However, whether sarcomere disassembly can *per se* trigger cell cycle re-entry remains unknown, a possibility that we have tested here. In this study, we have engineered a system to induce sarcomere disassembly in living murine cardiomyocytes based on the specific cleavage of the structural protein titin by tobacco etch virus protease. Although isolated neonatal cardiomyocytes with disassembled sarcomeres remain viable and retain low-amplitude contractile activity, our results show no evidence of increased cardiomyocyte proliferation in targeted cells, as indicated by the analyses of markers of DNA synthesis and cytokinesis. We obtain equivalent results when titin is cleaved in cardiomyocytes stimulated with mitogenic factors *in vitro* and in the adult myocardium *in vivo*. These findings suggest that the removal of sarcomere structural barriers is necessary, but not sufficient, for cardiomyocyte proliferation, which implies that additional factors are required for cardiomyocytes to undergo cell division.

Heart failure, a leading cause of morbidity and mortality worldwide, is mostly the long-term consequence of conditions causing massive and irreversible loss of cardiomyocytes, such as myocardial infarction (1). To improve clinical outcomes in these conditions, extensive efforts are being directed to promote cardiac regeneration through the induction of proliferation of surviving cardiomyocytes (2). However, this endeavor faces significant challenge. Whereas mammalian cardiomyocytes do proliferate during embryonic and fetal development, the vast majority of them exit the cell cycle within the first few days/weeks after birth and remain persistently refractory to proliferation from that moment onwards (3–5). Indeed, the natural response of adult mammalian hearts to cardiomyocyte loss is to replace necrotic tissue by a fibrotic scar and to induce hypertrophic growth of the remaining cardiomyocytes, which however typically fail to restore global contractile function (6, 7).

Different from mammals, the heart from a number of vertebrates, including zebrafish, newts, and axolotls, can regenerate completely after injury *via* the activation of cardiomyocyte proliferation (8–10). Based on these observations and on evidence that a limited fraction of mammalian cardiomyocytes can re-enter the cell cycle to some degree after myocardial injury (11, 12), several groups have identified a few pathways and molecules that induce proliferation of adult murine cardiomyocytes correlating with improved cardiac function following myocardial infarction (13–18). Disassembly of sarcomeres, the contractile units of terminally differentiated cardiomyocytes (19), is a feature common to both natural and induced cardiomyocyte proliferation (20) (Fig. 1*A*). Importantly, sarcomere disassembly is required for cardiomyocytes to proliferate, since inhibition of actin-capping adducin proteins or MMP-2 protease, two mediators of sarcomere disassembly, blunts cardiomyocyte proliferation (21, 22). These results support the traditional view that the dense arrays of sarcomeres in cardiomyocytes (*i.e.* the myofibrils) are an intrinsic barrier to cell division, potentially involving crosstalk with other cytoskeletal components and mitogenic signaling pathways (20).

Here, we hypothesized that the sole disassembly of sarcomeres could be enough to promote cardiomyocyte proliferation (Fig. 1*A*). In support of this hypothesis, cardiomyocytes devoid of sarcomeres are more proliferative (23), soft extracellular matrices disorganize sarcomeres and induce cardiomyocyte cell-cycle re-entry (24), and overexpression of adducin proteins can trigger sarcomere disassembly in cardiomyocytes correlating with increased levels of proliferation markers (22). Based on data that severing titin, a central

* For correspondence: Maria Rosaria Pricolo, mrpricolo@cnic.es; Jorge Alegre-Cebollada, jalegre@cnic.es.

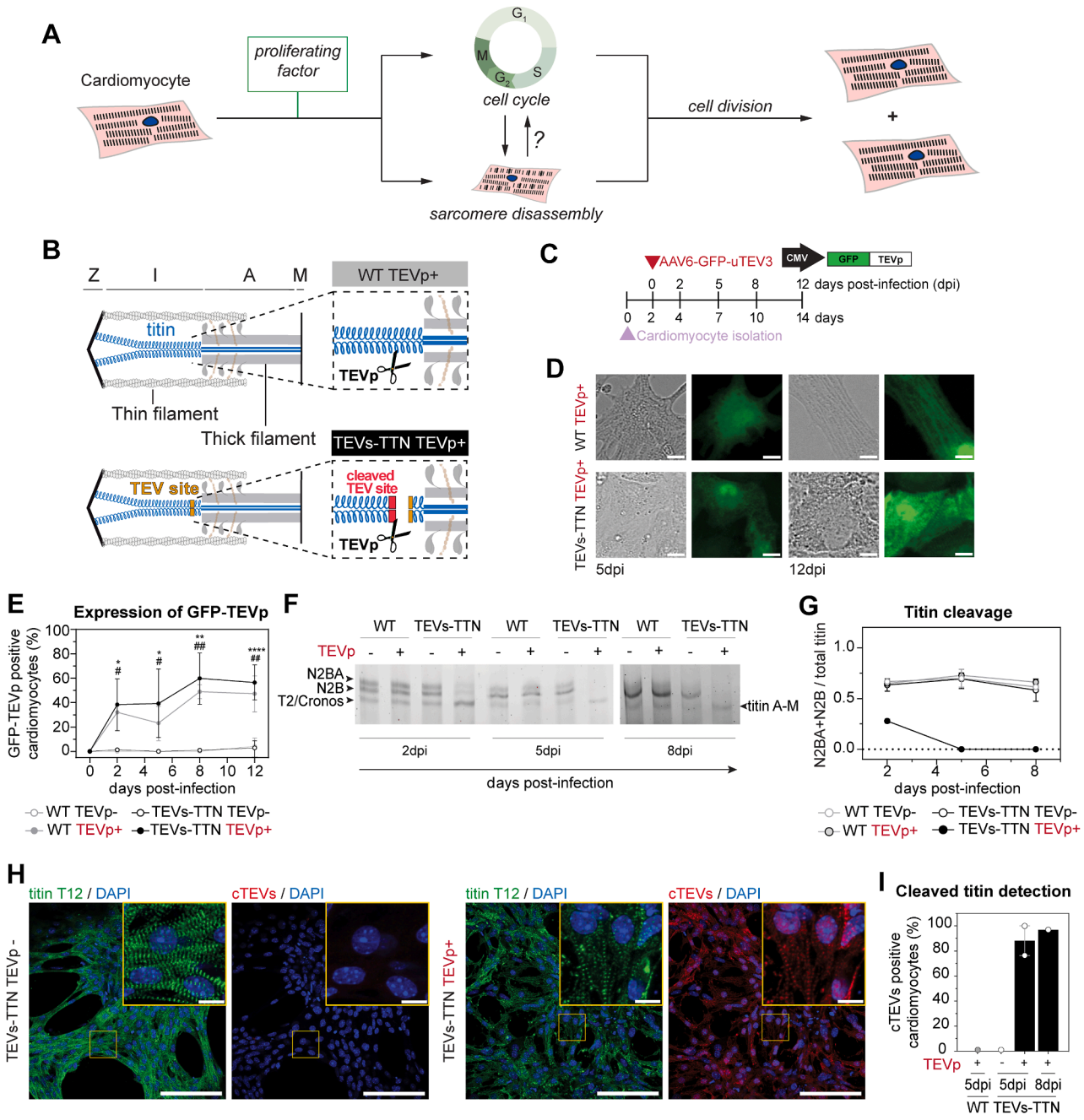

Figure 1. TEVp-induced cleavage of titin in living cardiomyocytes *in vitro*. *A*, scheme of cardiomyocyte proliferation, which requires cell cycle progression and sarcomere disassembly. This work examines whether sarcomere disassembly is enough to trigger progression in cell cycle. *B*, schematic representation of the titin cleavage strategy. TEVp recognizes the knocked-in TEVs within the I-band of titin in TEVs-TTN cardiomyocytes and cleaves titin. In contrast, titin remains uncleaved in WT cells. *C*, experimental design. Upon isolation, neonatal mouse cardiomyocytes are infected *in vitro* with GFP-TEVp–expressing AAV6 particles and analyzed at different days post infection. *D*, bright-field (*left*) and epifluorescence (*right*) representative images of living neonatal cardiomyocytes. Scale bars represent 10 μm. *E*, TEVp expression quantification from native GFP fluorescence (WT N = 3–4 isolations of cardiomyocytes; TEVs-TTN N = 4–8 isolations of cardiomyocytes). # indicates the statistical test for WT; * indicates the statistical test for TEVs-TTN. *F*, 1.8% polyacrylamide SDS-PAGE electrophoresis to analyze titin content. *G*, quantification of the proportion of the N2BA and N2B titin bands with respect to all titin bands (N = 2–3 isolations of cardiomyocytes). *H*, detection and (*I*) quantification of cleaved titin with anti cTEVs. (N = 1–2 isolations of cardiomyocytes). Scale bars represent 100 μm. ROI scale bars represent 10 μm. Results are plotted as mean ± standard deviation (SD). Statistical significance is calculated using unpaired Student's *t* test. *p*-value <0.05 (*/#), <0.01 (**/##), <0.0001 (****).

structural component of myofibrils (25, 26) (Fig. 1*B*), destabilizes skeletal muscle sarcomeres (27, 28), we set out to investigate whether titin cleavage could be exploited to elicit sarcomere disassembly and subsequent proliferation of targeted cardiomyocytes. In most of our experiments, we focused on *in vitro* experiments using neonatal cardiomyocytes due to their basal intrinsic proliferative capacity. In addition, we have also done complementary assays *in vivo*

to broaden the scope of our conclusions. Our results demonstrate that full titin cleavage does indeed cause sarcomere disassembly in otherwise viable cells; however, contrary to our motivating hypothesis, we find no evidence of increased proliferation of cardiomyocytes containing cleaved titin.

Results

Induction of specific titin cleavage in living cardiomyocytes

For our experiments, we exploited a homozygous knock-in mouse model that contains a recognition site for tobacco etch virus protease (TEVp) in the elastic I-band region of titin (TEVs-TTN mice) (29) (Fig. 1*B*). The ability of TEVp to cleave cardiac titin from TEVs-TTN sarcomeres has been demonstrated adding purified TEVp to demembranated preparations (27, 29, 30). Here, to implement titin cleavage in living cells, we first infected *in vitro* neonatal TEVs-TTN cardiomyocytes with AAV6 viral particles expressing different forms of TEVp under the control of the constitutive cytomegalovirus (CMV) promoter. Among the four different TEVp constructs tested, we find optimal expression and cytosolic localization of GFP-uTEV3 (hereafter referred to as GFP-TEVp), which contains an improved version of TEVp obtained by directed evolution (31) (Fig. S1*A*). We used GFP-TEVp–expressing AAV6 particles for all subsequent experiments.

We tracked expression of GFP-TEVp in both WT and TEVs-TTN neonatal cardiomyocytes *in vitro* at different days post infection (dpi). In both genotypes, GFP-positive cells are already evident at 2 dpi reaching ∼60% of cardiomyocytes from 8 dpi (Figs. 1, *C–E* and S1*B*). Next, we examined the levels of titin cleavage by 1.8% polyacrylamide SDS-PAGE electrophoresis. As expected, in all WT and untreated TEVs-TTN control cells, we detect three major titin bands corresponding to full-length N2BA and N2B isoforms and the higher electrophoretic-mobility band originating from the Cronos isoform and/or the T2 degradation fragment (26) (Fig. 1*F*). In contrast, AAV-infected TEVs-TTN samples show just one major titin band of electrophoretic mobility compatible with the C-terminal titin fragment derived from TEVp activity (29) (A-M titin, similar mobility to Cronos/T2, Fig. 1*F*). Quantification demonstrates that full-length titin is completely absent in TEVs-TTN samples from 5 dpi (Fig. 1*G*). In agreement with this result, from this time point, the vast majority of TEVs-TTN cardiomyocytes (identified as cells showing titin staining with T12 antibody (32)) are also positive for anti-cleaved TEVs (cTEVs) antibody (28) (Fig. 1, *H* and *I*), which highlights limited sensitivity of GFP-TEVp detection by epifluorescence (Fig. 1*E*).

In combination, our results demonstrate successful implementation of titin cleavage in living cardiomyocytes *in vitro*. Severing of titin is complete even at low GFP-TEVp levels that cannot be detected by conventional epifluorescence, illustrating the catalytic nature of our protease-based approach. Importantly, we find no effects of GFP-TEVp expression in cardiomyocytes that are devoid of the TEVp recognition site in titin, which supports the specificity of the phenotypes we detect upon GFP-TEVp expression in TEVs-TTN cardiomyocytes.

Sarcomere disassembly upon titin cleavage in otherwise viable cardiomyocytes

Having verified the full cleavage of titin in AAV-infected TEVs-TTN cardiomyocytes *in vitro* (as opposed to limited cleavage in the equivalent *in vivo* system(33)), we next examined the structural integrity of targeted sarcomeres the *in vitro* system. Z-disk staining with T12 anti-titin antibody indicates loss of normal sarcomere pattern in AAV-infected TEVs-TTN cardiomyocytes, but not in any of the three control groups (Figs. 2, *A* and *B* and S2*A*). We quantified sarcomere disassembly using an automatic analysis of the anisotropy of T12 fluorescence signal (Figs. 2*C* and S2*B*) and by blinded inspection of fluorescence images to classify structural integrity of sarcomeres (Fig. 2*D*). Although analysis of anisotropy appears to be less sensitive to capture differences between groups (Fig. 2*C*), probably because the fluorescence pattern of fully disassembled sarcomeres is not isotropic (Fig. 2*B*), both analyses readily capture progressive sarcomere disorganization in AAV-infected TEVs-TTN cardiomyocytes (Fig. 2, *C* and *D*). Indeed, most TEVs-TTN cardiomyocytes in the AAV-infected group show at least partially disassembled sarcomeres already at 2 dpi; no intact sarcomeres are detected in this experimental group at 8 dpi (Fig. 2*D*).

We extended our analysis to other relevant components of the sarcomere (Fig. 3*A*). Similar to T12 staining, Z-disk scaffold α-actinin shows a disorganized, nonsarcomeric pattern resembling disconnected Z-bodies already at 2 dpi (21) (Figs. 3*B* and S2*C*). Staining of troponin T, a thin filament component, is also devoid of striated pattern in AAV-infected TEVs-TTN cardiomyocytes, although in this case, remnant fibrillar structures are seen even at 8 dpi (Figs. 3*B* and S2*C*). Finally, targeted cardiomyocytes show diffuse staining of the TTN-9 M-band titin epitope (Fig. 3*C*).

We asked ourselves whether sarcomere disassembly upon titin cleavage affects cardiomyocyte viability in our *in vitro* system. Using the 3-[4,5-dimethylthiazol-2-yl]-2,5 diphenyl tetrazolium bromide (MTT) assay, we find no evidence of altered metabolic activity in TEVp-expressing TEVs-TTN cardiomyocytes at 5 dpi, a time point where titin cleavage is complete (Fig. 1*G*) and intact sarcomeres are scarce (Fig. 2*D*), despite some nonspecific effects could have been expected according to results with WT counterparts (Fig. 4*A*). Similarly, we detect no indication of apoptosis using terminal deoxynucleotidyl transferase dUTP nick end labeling (TUNEL) assays at 5 dpi (Fig. 4*B*). Furthermore, tracking spontaneous cardiomyocyte contractility by light microscopy (Fig. 4, *C* and *D*), we observe that most AAV-infected TEVs-TTN cardiomyocytes are able to beat, although with much reduced amplitude as expected from the observed loss of sarcomeres (Fig. 4, *E* and *F* and Videos S1 and S2). This effect is accompanied by lower duration of contractions at longer time points (Fig. 4*G*).

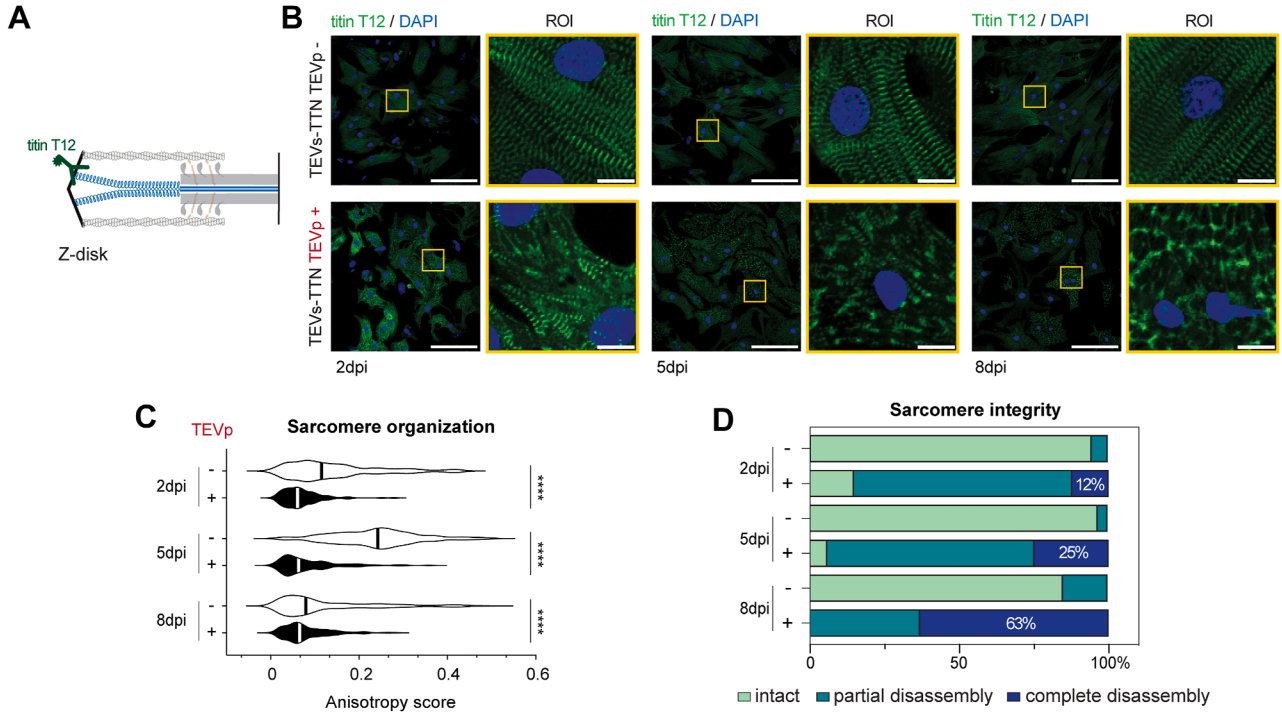

Figure 2. Sarcomere disassembly upon titin cleavage *in vitro*. *A*, the T12 titin epitope localizes to the Z-disk of sarcomeres. *B*, representative immunofluorescence images of TEVs-TTN cardiomyocytes expressing or not GFP-TEVp. Scale bars represent 100 μm. ROI scale bars represent 10 μm. *C*, sarcomere organization quantified as anisotropy of T12 signal in immunofluorescences (N = 2–3 isolations of cardiomyocytes). The position of the mean value within Violin plots is indicated. *D*, qualitative estimation of sarcomere integrity (N = 2 isolations of cardiomyocytes). Statistical significance is calculated using unpaired Student's *t* test. *p*-value <0.0001 (****).

In summary, we find that titin cleavage *in vitro* induces progressive disassembly of sarcomeric components in the absence of noticeable cell death. In addition, targeted cardiomyocytes retain measurable contractile activity.

Invariant proliferation of cardiomyocytes containing cleaved titin

So far, our data demonstrate that full titin cleavage causes sarcomere disassembly without compromising the global viability of targeted cardiomyocytes. To assess whether titin-cleavage–induced sarcomere disassembly triggers cardiomyocyte proliferation, we measured several markers of cell cycle upon titin cleavage *in vitro* (Fig. 5*A*). Specifically, we studied nuclear incorporation of 5-ethynyl-2′-deoxyuridine (EdU) (Figs. 5*B* and S3, *A* and *B*) and presence of Aurora B (Figs. 5*C* and S3, *A* and *B*) as markers of DNA synthesis and mitosis, respectively (34). Quantification indicates that expression of GFP-TEVp does not alter EdU nuclear incorporation (Fig. 5*D*) nor the proportion of Aurora B positive cardiomyocytes (Fig. 5*E*). Accordingly, we observe that the fraction of binucleated AAV-infected TEVs-TTN cardiomyocytes is comparable to that of the controls (Fig. 5, *F* and *G*). Altogether, our results indicate that titin-induced sarcomere disassembly does not promote proliferation of neonatal cardiomyocytes *in vitro*.

To examine whether our results could be extended to the *in vivo* situation, we also investigated the effect of titin cleavage on adult cardiomyocyte proliferation by expressing GFP-TEVp in the myocardium of 9-19-week-old WT and TEVs-TTN mice (Fig. 5*H*) under conditions that result in different levels of sarcomere disassembly in 30% of the cardiomyocytes in TEVs-TTN mice (33). As expected, proliferation analysis using Ki-67 as a cell cycle marker (35) shows less than 0.05% proliferative adult cardiomyocytes in basal conditions; this fraction is not affected by the expression of GFP-TEVp (Fig. 5, *I* and *J*, S4*A*). To directly address whether sarcomere disassembly affects cardiomyocyte cell cycle activity at the single-cell level *in vivo*, we quantified Ki-67 expression specifically in cardiomyocytes containing cleaved titin (cTEVs-positive) in GFP-TEVp–expressing hearts and compared results with neighboring cTEVs-negative cardiomyocytes. Results indicate that the percentage of Ki-67–positive nuclei does not significantly differ between cTEVs-negative and cTEVs-positive cardiomyocytes (Fig. S4, *B* and *C*). Hence, both our *in vitro* and *in vivo* data suggest that titin-cleavage–induced sarcomere disassembly does not lead to cardiomyocyte proliferation.

As an orthogonal approach, we analyzed available RNAseq data in the quest of proliferative signals that could be detectable at the transcriptional level. Specifically, we checked if genes belonging to Gene Ontology (GO) terms related to cardiac cell proliferation are differentially expressed upon titin cleavage *in vitro*. Among the 270 differentially expressed genes (DEGs) in AAV6-infected TEVs-TTN neonatal cardiomyocytes at 5 dpi compared to WT cells (33), we only find

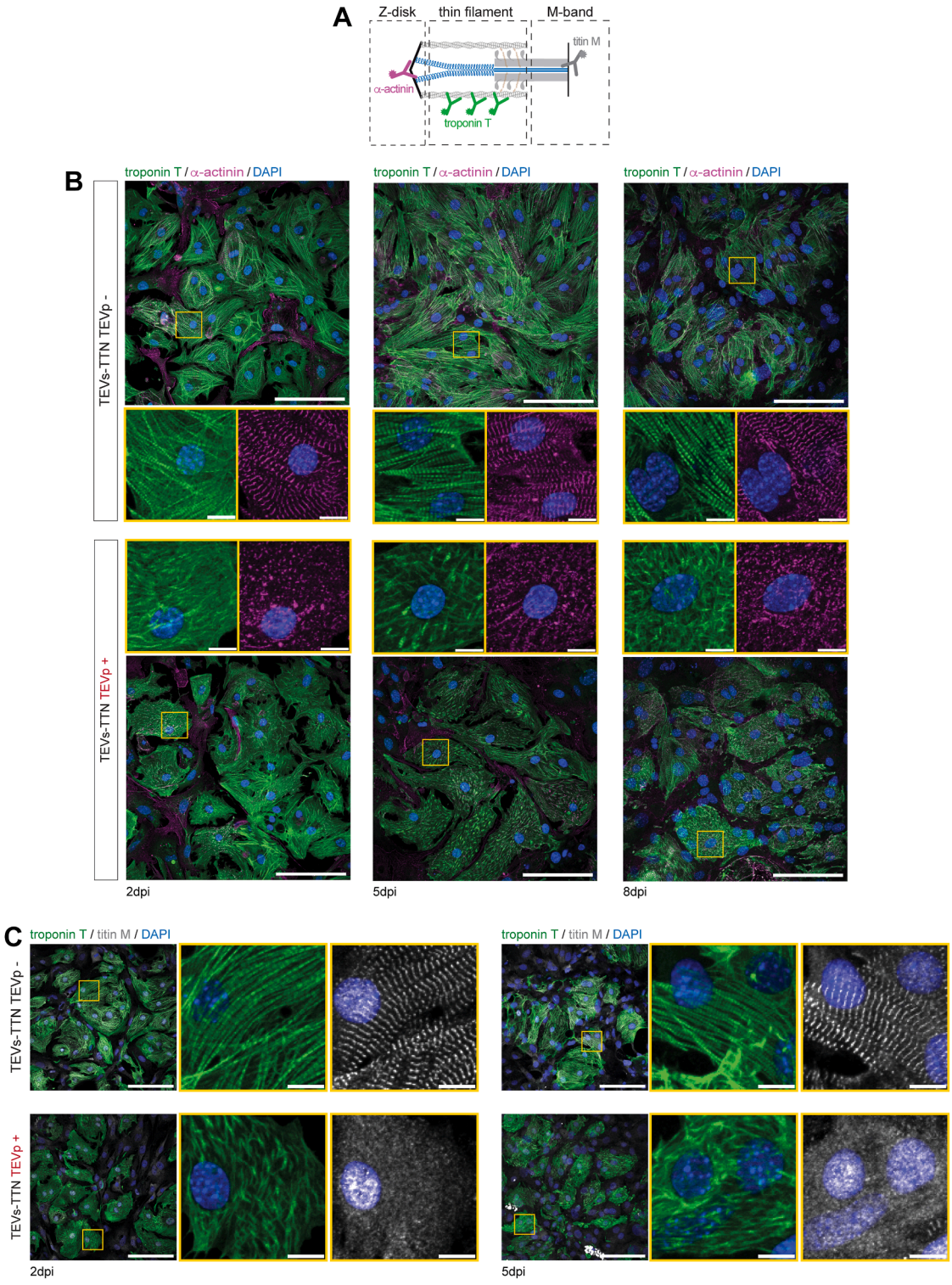

Figure 3. Thin filament and M-line disassembly upon titin cleavage *in vitro*. *A*, sarcomere epitopes used in immunofluorescence imaging to investigate sarcomere disarray. *B* and *C*, representative immunofluorescence images of TEVs-TTN cardiomyocytes expressing or not GFP-TEVp. Scale bars represent 100 μm. ROI scale bars represent 10 μm.

one gene belonging to GO0060038 (cardiac cell proliferation) but none in related terms including GO0060045 (positive regulation of cardiac muscle cell proliferation) and GO0060043 (*regulation of cardiac muscle cell proliferation*). In a more sensitive RNA seq analysis of the titin-cleavage model *in vivo*, which captures 3220 DEGs in infected *versus* control TEVs-TTN myocardium (33); results also indicate a residual contribution of genes related to cardiomyocyte proliferation. Specifically, only 10 (0.3%), 15 (0.4%), and 8 (0.2%) DEGs fall in the GO0060045, GO0060043, and GO0060038

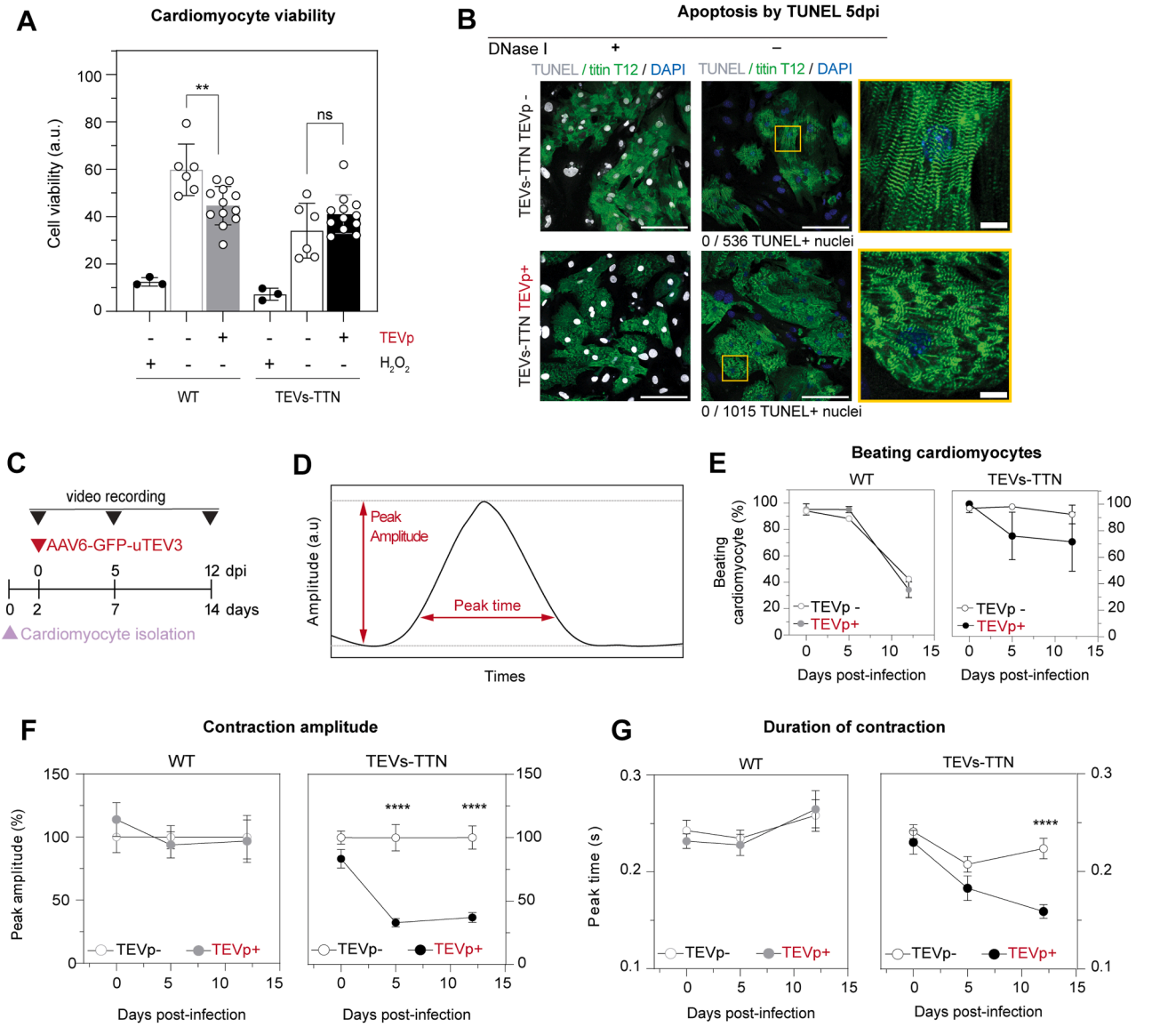

Figure 4. Beating alteration in GFP-TEVp–expressing TEVs-TTN cardiomyocytes *in vitro* in the absence of cell death. *A*, cardiomyocyte viability determined *via* the MTT assay at 5 dpi. Cells incubated with hydrogen peroxide (H_2O_2) are used as positive control (N = 1 isolation of cardiomyocytes; n = 3–12 technical replicates). Results are plotted as mean ± standard deviation (SD). *B*, representative images of TEVs-TTN cardiomyocyte apoptosis detected by TUNEL. Positive control samples are incubated with DNase I. Scale bars represent 100 μm. ROI scale bar represents 10 μm. *C*, schematic of experiment to monitor cardiomyocyte contraction. 0 dpi samples were measured before infection. *D*, peak amplitude and time are analyzed with MYOCYTER (50). *E*, fraction of spontaneously beating WT (*left*) and TEVs-TTN (*right*) cardiomyocytes, expressing or not GFP-TEVp (N = 3 isolations of cardiomyocytes). *F*, contraction amplitude of WT (*left*) and TEVs-TTN (*right*) cardiomyocytes, expressing or not GFP-TEVp (N = 3 isolations of cardiomyocytes). *G*, duration of contraction of WT (*left*) and TEVs-TTN (*right*) cardiomyocytes, expressing or not GFP-TEVp (N = 3 isolations of cardiomyocytes for panels *E*–*G*). Results are plotted as mean ± standard error of the mean (SEM). Statistical significance is calculated using unpaired Student's *t* test. *p*-value <0.005 (**), <0.0001 (****). non-significant (ns).

terms, respectively. Hence, our analyses indicate no transcriptional signatures of cardiomyocyte proliferation upon cleavage of titin.

Sarcomere disassembly does not enhance mitogen-induced proliferation

To determine whether sarcomere disassembly can boost cardiomyocyte proliferation under proproliferative conditions, we stimulated cardiomyocyte cell cycle activity using active version of the Hippo pathway effector Yap, Yap5SA, or using the transcription factor c-Myc (36, 37). Neonatal cardiomyocytes were infected *in vitro* with the AAV6 vector expressing GFP-TEVp alone or in combination with vectors expressing Yap5SA or c-Myc (Fig. 6*A*). As expected, expression of Yap5SA or c-Myc alone significantly increased EdU incorporation (Fig. 6, *B* and *C*) and AuroraB-positive nuclei (Fig. 6, *B* and *D*) and compared with control conditions. Consistent with our previous experiments, co-expression of GFP-TEVp with either Yap5SA or c-Myc did not further enhance proliferation relative to mitogens stimuli alone. Analysis of sarcomere organization confirmed robust sarcomere disassembly in cardiomyocytes expressing TEVp, both

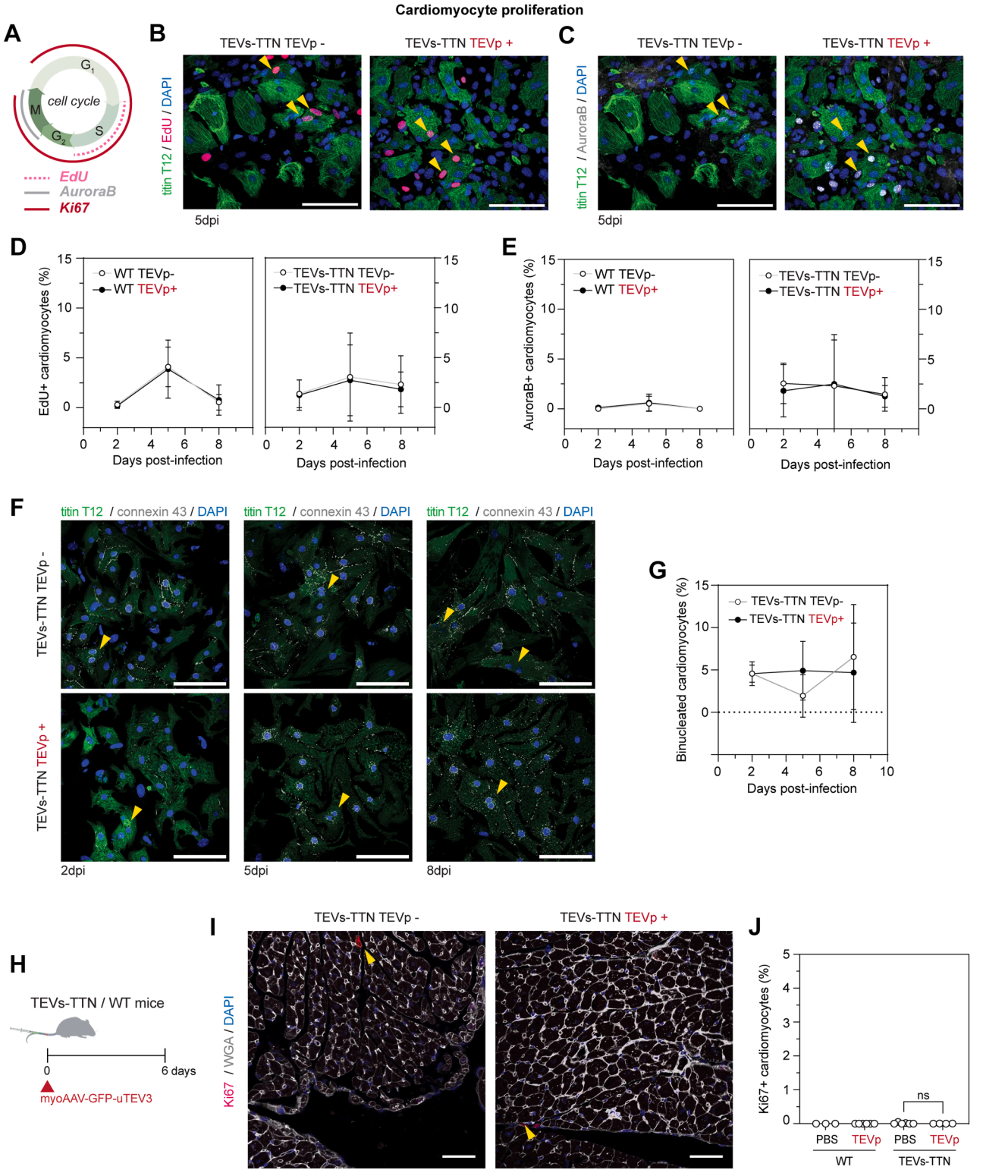

Figure 5. Examination of cardiomyocyte proliferation markers. *A*, schematic representation of markers of different stages of the cell cycle. *B*, representative images of EdU (*red*) incorporation in TEVs-TTN cardiomyocytes nuclei (*yellow arrowheads*) in samples infected or not with GFP-TEVp-expressing AAV6 vectors *in vitro*. Scale bars represents 100 μm. *C*, representative images of Aurora B (*gray*)-positive nuclei in TEVs-TTN cardiomyocytes (*yellow arrowheads*) expressing or not with GFP-TEVp *in vitro*. Scale bars represent 100 μm. *D*, quantification of EdU incorporation in WT (*left*) and TEVs-TTN (*right*) cardiomyocytes expressing or not GFP-TEVp (WT N = 3 isolations of cardiomyocytes; TEVs-TTN N = 4 isolations of cardiomyocytes) *in vitro*. *E*, quantification of Aurora B-positive WT (*left*) and TEVs-TTN (*right*) cardiomyocytes expressing or not GFP-TEVp *in vitro* (WT N = 2 isolations of cardiomyocytes; TEVs-TTN N = 3 isolations of cardiomyocytes). *F*, representative images showing binucleated TEVs-TTN cardiomyocytes (*yellow arrow heads*) *in vitro*. Scale bars represent 100 μm. Panel TEVs-TTN TEVp+ 2dpi is the same as Figure 2*B*. *G*, quantification of binucleated TEVs-TTN cardiomyocytes *in vitro* (N = 2–3 isolations of cardiomyocytes). *H*, schematic representation of titin-cleavage induction *in vivo*. *I*, representative immunodetection of Ki67 proliferation marker in ventricular myocardium of TEVs-TTN mice expressing or not GFP-TEVp. Scale bars represent 50 μm. *J*, quantification of Ki67-positive cardiomyocytes in ventricular myocardium (N = 3–6 mice). Results are plotted as mean ± standard deviation (SD). Statistical significance is calculated using unpaired Student's *t* test. non-significant (ns).

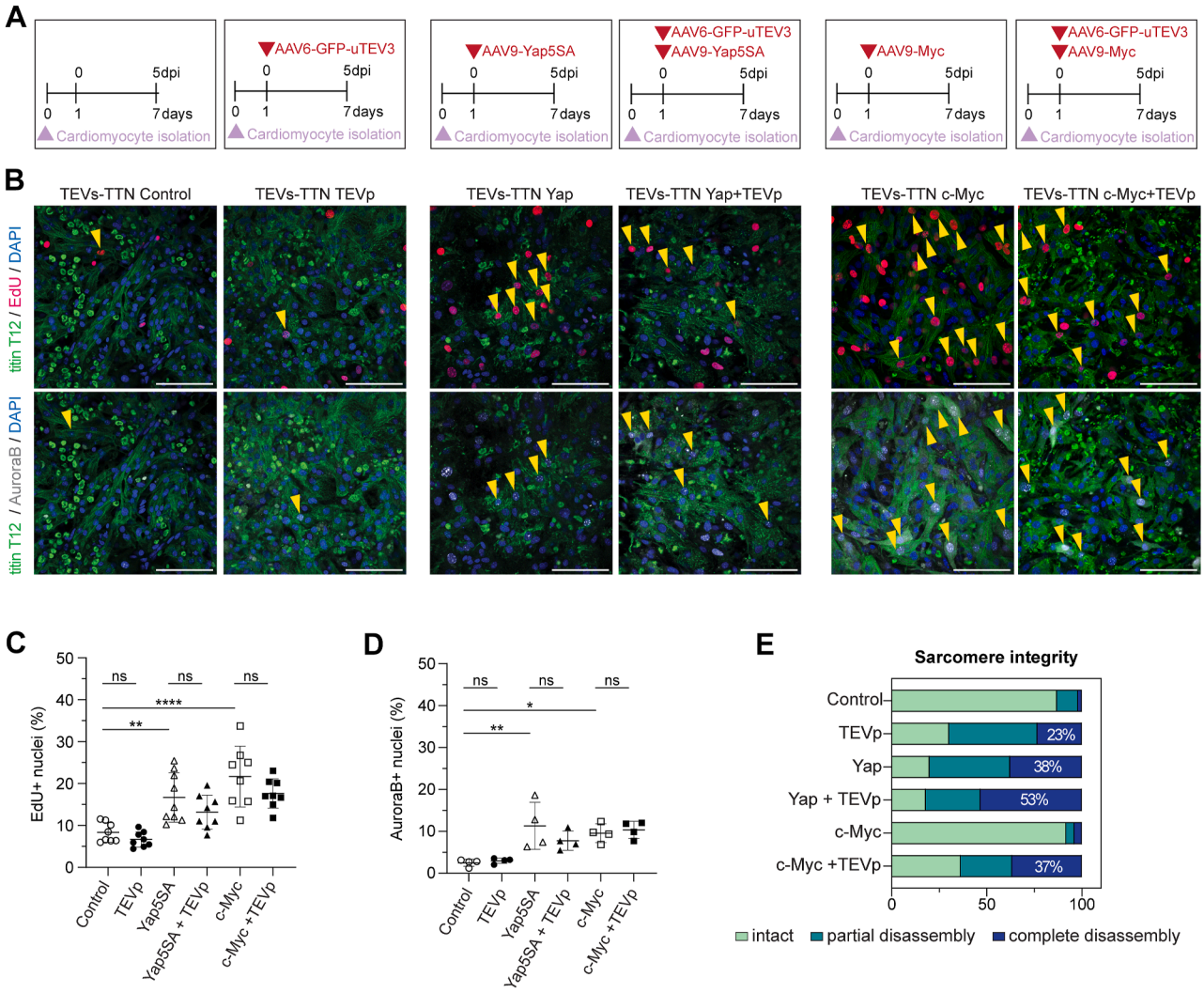

Figure 6. Concurrent cell cycle stimulation and titin-induced sarcomere disassembly. *A*, experimental design. *B*, representative images highlight with *yellow arrowheads* EdU (*red*) incorporation and Aurora B (*gray*)-positive nuclei in TEVs-TTN cardiomyocytes in samples expressing TEVp, Yap5SA, c-Myc, or a combination of Yap5SA or c-Myc and TEVp. Scale bars represent 100 μm. *C*, quantification of EdU incorporation (N = 1 isolation of cardiomyocytes, n = 8–9 images from two independent infections). *D*, quantification of Aurora B-positive nuclei (N = 1 isolation of cardiomyocytes, n = 4 images). *E*, qualitative estimation of sarcomere integrity (N = 1 isolations of cardiomyocytes, n = 2 from two independent infections). Results are plotted as mean ± standard deviation (SD). Statistical significance is calculated using one-way ANOVA. non-significant (ns), *p*-value <0.05 (*), <0.01 (**), <0.0001 (****).

alone and in combination with Yap5SA or c-Myc (Fig. 6*E*). In combination, these data indicate that sarcomere disassembly induced by titin cleavage does not potentiate cardiomyocyte proliferation even in the presence of strong proliferative stimuli *in vitro*.

Discussion

The cardiac muscle has limited capacity for renewal, which results in important functional deficits in the many sick hearts that experience loss of cardiomyocytes, regardless of the underlying etiology (38, 39). Opening new windows of opportunity to treat these highly prevalent heart diseases, in recent years several factors have been identified that can stimulate cardiomyocyte proliferation and promote cardiac regeneration, including inhibitors of cell signaling pathways, growth factors, and miRNAs (13–18). A common feature of cardiomyocyte division triggered by these factors, very much resembling natural cardiomyocyte proliferation, is the induction of a more dedifferentiated state of cardiomyocytes that includes disassembly of sarcomeres. Indeed, sarcomere disassembly itself has even been proposed to be a *bona fide* regulator of cell cycle progression (20). Supporting this mechanistic role, overexpression of actin-capping adducin proteins induces sarcomere disassembly that, under some conditions, correlates with increased cardiomyocyte proliferative capacity (22). Considering these results, we reasoned that the potential for cardiomyocyte regeneration could be also unlocked by sarcomere disassembly resulting from titin cleavage. Although our work does indeed demonstrate that titin cleavage causes disassembly of sarcomeres in the absence of noticeable cell stress or death, we find no evidence of

accompanying proliferation of targeted neonatal cardiomyocytes *in vitro*, even when subjected to mitogenic stimuli, or adult counterparts *in vivo*. It is possible that increasing the number of targeted cardiomyocytes *in vivo* may result in better sensitivity to capture proliferating cardiomyocytes; however, the extensive induction of myocardial remodeling and heart failure triggered by further titin cleavage could also block cardiomyocyte proliferation (33).

The mechanisms driving sarcomere disassembly during mammalian cardiomyocyte proliferation remain largely unknown although they seem to be adapted to the physiological state of cells (*i.e.* different mechanisms in, for example, embryonic *versus* neonatal cardiomyocytes) (20, 22, 40). In our experiments, extensive titin cleavage is detected in GFP-TEVp–expressing TEVs-TTN neonatal cardiomyocytes as early as 2 dpi (Fig. 1, *F* and *G*). At this time, disassembly of the Z-disk into structures resembling Z-bodies is already evident, as shown by the location of α-actinin in immunofluorescence (Fig. 3). Similarly, troponin T staining reveals disassembly of thin filaments in GFP-TEVp–expressing TEVs-TTN cardiomyocytes, although the distribution of the protein in targeted cells remains more fibrillar-like than for the other sarcomeric proteins we have studied (Figs. 2 and 3). From 5 dpi, we find complete titin cleavage correlating with higher proportion of fully disassembled sarcomeres (Fig. 1, *F* and *G* and 2*D*). Intriguingly, T12 staining, which labels the Z-disk portion of titin, shows in targeted cells a nonsarcomeric pattern that is distinct from α-actinin's (Figs. 2 and 3). This observation suggests that Z-disk protein complexes dissociate upon titin cleavage and that the resulting protein components localize to different regions of the cell. A similar situation is observed for the titin fragments originating from GFP-TEVp activity (compare the diffuse M-band and spotted Z-disk stainings of titin in AAV-infected TEVs-TTN cardiomyocytes, Figs. 2*B* and 3*C*). Remarkably, different location of titin regions is also detected during natural disassembly of sarcomeres in cycling embryonic cardiomyocytes (41). In this regard, it is hard to conceive how titin Z-disk and M-line titin epitopes, even if distant, can show different subcellular localization in cardiomyocytes undergoing metaphase without invoking proteolysis of titin (41). In fact, several proteases targeting titin have been proposed to contribute to sarcomere disassembly (20). Among them, MMP-2 has been identified as a fundamental mediator of oncostatin M–induced sarcomere disassembly and cardiomyocyte proliferation (21, 42). Remarkably, oncostatin M induces loss of striated pattern of both Z-disk and M-line regions of the sarcomere in a highly similar manner to the one we detect upon GFP-TEVp–mediated titin cleavage.

In combination our results indicate that titin-cleavage–induced sarcomere disassembly, despite not triggering cardiomyocyte proliferation, does recapitulate features that are also observed in proliferating cardiomyocytes. Whether proteolysis of sarcomeric components is required for sarcomere disassembly and cardiomyocyte proliferation remains controversial (21, 40, 41). Arguably, extensive proteolysis would require rapid and energy-costing re-synthesis of sarcomeric components to limit the loss of contractile function of the myocardium. Our work adds a relevant counter-argument in this regard, since we demonstrate that just a single proteolytic cut in titin is enough to trigger sarcomere disassembly. Considering the well-known cardiac titin isoform switch that happens during late embryonic/early postnatal development (43), it is tempting to speculate that titin cleavage during these proliferative stages could contribute to sarcomere disassembly of dividing cardiomyocytes while ensuring replacement of titin isoforms.

Importantly, our model of titin-cleavage–induced sarcomere disassembly also results in concomitant reduction of cardiomyocyte-cardiomyocyte adhesion strength and alteration of connexin 43 localization (Fig. 5*F*, more extensive analysis *in vitro* and *in vivo* in (33)). Connexin 43 is the main component of gap junctions within intercalated discs, complex structures responsible for rapid and coordinated electromechanical coupling between neighboring cardiomyocytes (44). Since cell–cell contacts appear to be preserved in naturally cycling cardiomyocytes (41), the possibility exists that loss of cell adhesion upon titin cleavage somehow opposes cell proliferation in our model. Considering our results, it will be interesting to investigate why sarcomere disassembly in naturally proliferating cardiomyocytes does not compromise cell adhesion as we have detected here. A contributing factor may be that cardiomyocytes undergoing natural cell division are surrounded by several counterparts with intact sarcomeres unlike in our *in vitro* experiments. Also, considering that cardiomyocytes containing cleaved titin retain some contractile activity and that residual thick filament structure could block proliferation (41), it will be interesting to study how the thick filament is affected by titin cleavage.

In conclusion, our work demonstrates that cleaving titin is sufficient to induce sarcomere disassembly in living cardiomyocytes. However, the lack of ensuing cardiomyocyte proliferation suggests that sarcomere disassembly *per se* is not sufficient to trigger cell cycle entry nor does it potentiate the proliferative response induced by mitogenic signals.

Experimental procedures

Animal experimentation

Animals were handled in accordance with European and Spanish guidelines for animal welfare and with the recommendations in the Guide for the Care and Use of Laboratory Animals of the National Institutes of Health. The protocol was approved by the Ethics Committee of Animal Experiments of our institutional committees (project numbers PROEX 042/18 and PROEX 107.8/23). Neonates were used in our experiments with no consideration of sex. Only male mice were used for *in vivo* experiments.

Adeno-associated virus production

Different TEVp constructs were expressed in adeno-associated virus (AAV) under the control of the CMV promoter. Specifically, AAV-compatible vectors CMV-mCherry-TEV and CMV-Tomato-TEV were from Addgene

(#58868 and #58872, respectively). Plasmids CMV-GFP-uTEV3 and CMV-mCherry-uTEV3 encoding an improved TEVp variant were produced by us and can be obtained from Addgene (#234320 and #238000, respectively) (31). AAV plasmid encoding for Yap5SA was kindly donated by the group of Eldad Tzahor, whereas the AAV plasmid encoding for c-Myc overexpression under CMV promoter was designed and constructed using VectorBuilder design studio. Production and quantification of AAV serotype 6, AAV serotype 9, and AAV-MYO (45) particles have been described elsewhere (28, 33). Titers are reported as viral genomes per milliliter (vg/ml).

Cardiomyocyte isolation and infection

Neonatal mouse cardiomyocytes were isolated from WT and TEVs-TTN mice. Dissected hearts from neonatal (P1-3) were minced with a scissor in cold Hanks' Balanced Salt Solution and dissociated using the Pierce Primary Cardiomyocyte Isolation Kit (Thermo Fisher ScientificPierce, 88281) in 0.21 ml enzyme mix/heart in a 2 ml reaction tube for 20 min at 37 °C with occasional gentle shaking. The pellet was centrifuged, washed twice with Hanks' Balanced Salt Solution, and resuspended in 0.5 ml cardiomyocyte medium (Dulbecco's Modified Eagle Medium for Primary Cell Isolation containing 10% heat-inactivated Fetal Bovine Serum and 1% penicillin/streptomycin) per heart and plated onto MatTek dishes covered with matrigel solution (Thermo Fisher Scientific, 11553620). Cardiomyocytes were infected overnight with AAV6-expressing TEVp, AAV9-expressing Yap5SA (36), and AAV9-expressing c-Myc (37) constructs 24 to 48 h after plating (at a multiplicity of infection of 500,000).

Mice systemic injections and cardiac tissue processing

WT and homozygous TEVs-TTN mice were injected with AAVMYO viral particles or 100 µl PBS, 0.001% pluronic acid *via* the tail vein. The mice were randomly injected to avoid differences arising from the skill of the researcher to inject. Mice were then returned to their breeding cages until sacrifice by CO2 inhalation 6 dpi. Upon sacrifice, the heart together with the ascending aorta and pulmonary trunk were dissected out. The ascending aorta, from the sinotubular junction to the branching of the brachiocephalic artery and atrial myocardium were excised and discarded. Transverse ventricular samples were obtained, and the upper region of both ventricles was fixed in 4% paraformaldehyde (PFA4%) overnight at 4 °C.

Cardiomyocyte live imaging

Isolated cardiomyocytes seeded in p35 culture plates (Mattek, P35G-0-10-C) were used for live imaging. After 2, 5, 8, and 12 dpis, the culture media were replaced by DMEM without phenol red (Gibco, 31053028) containing 10% heat-inactivated FBS and 1% penicillin/streptomycin. Time-lapse imaging was performed at 37 °C and 5% CO_2 using a Plan Apo λ 20x/0.75 objective in a Nikon ECLIPSE Ti epifluorescence microscope coupled to an Orca ER Hamamatsu CCD camera. GFP-TEVp expression was quantified by capturing native green fluorescence.

Quantification of titin cleavage

2 × 10 (6) cardiomyocytes were seeded in p35 culture plates. Cell lysates were obtained in 150 µl of sample buffer (3% SDS, 50 mM Tris–Cl pH 6.8) supplemented with 50 mM N-ethylmaleimide (Sigma-Aldrich, E3876) and protease inhibitor Cocktail Set III (Millipore). Samples were diluted in 0.06% bromophenol blue and 10% glycerol and run on 1.8% polyacrylamide SDS-PAGE gels. Titin proteins were visualized by SYPRO Ruby staining (Thermo Fisher Scientific, S21900) and relative band intensities were measured using QuantityOne Software.

Immunocytochemistry and immunohistochemistry

Neonatal cardiomyocytes were fixed with 4% (v/v) PFA at room temperature (RT) for 10 min, permeabilized with 0.2% (v/v) Triton X-100 (Sigma-Aldrich) in 1% (w/v) Bovine Serum Albumin (BSA) (Sigma-Aldrich) for 5 min, and blocked in SB buffer (PBS containing 10% FBS and 1.5% BSA) for 1 h at RT. Following incubation with primary antibodies at 4 °C overnight, samples were incubated with secondary antibodies and 5 µg/ml 4′,6-diamidino-2-phenylindole dihydrochloride (DAPI) to mark the location of the nuclei at RT for 1 h (antibodies are reported in Table S1). Fluoromont G (bioNova, 0100-01) was used as mounting medium and allowed to cure overnight. Images were taken using confocal microscope Zeiss LSM700 with Plan-Apochromat 40x/1.3 Oil DIC M27. Regarding myocardial samples, ventricles were fixed in PFA overnight at 4 °C. After washing in PBS, the tissue was subsequently treated with 10% and 30% sucrose, embedded in optimum cutting temperature (Tissue-Tek Compound 4583, Sakura), and sectioned at 8 µm with a cryostat (Leica). Transverse sections of the middle portion of each segment were permeabilized with 0.3% Triton X-100 in PBS and blocked in SB buffer. Sections were first incubated with anti Ki67 at 4 °C overnight and after washing, they were incubated with the anti- rat IgG -Alexa Fluor 555 Plus and wheat germ agglutinin at RT for 1.5 h (Table S1). After the secondary antibody incubation, sections were stained with DAPI. Mowiol 4-88 (Sigma-Aldrich) was used as mounting medium and allowed to cure overnight. Images were taken using confocal microscope Nikon A1R with a Plan Apo 40x/1.3 Oil objective.

Image analysis

We used Fiji platform (46) and custom script plugins. To measure GFP-TEVp levels, cardiomyocytes were identified using sarcomere markers and were segmented manually. GFP-positive cells were counted, and regions containing green fluorescent cardiomyocytes were selected to measure GFP intensity. Sarcomere organization was estimated measuring anisotropy of T12 signal using FibrilTool (47). Only cardiomyocytes showing T12 staining were used in the

analysis of cell cycle markers *in vitro*. Binucleated cardiomyocytes were quantified based on the presence of double DAPI positive nuclei in manually segmented cells, using connexin 43 as a membrane marker. For TEVs-TTN-TEVp, which exhibit a reduction in connexin 43, cell segmentation is facilitated because cells have less intimate contacts with their neighbors (33). Ki67-positive cardiomyocytes in the myocardium were quantified using a custom script plugin building on the Cellpose plugin (48) for general cellular segmentation based on the wheat germ agglutinin membrane marker and the Stardist plugin (49) for nuclear segmentation. Cellular area larger than 50 μm^2 was used to quantify positive cardiomyocytes in transversal section. The quantification of Ki67-positive cardiomyocytes according to cTEVs signal was done manually.

Cardiomyocytes metabolic activity

Cardiomyocyte viability was examined using the MTT assay (Roche, 11465007001). Briefly, neonatal cardiomyocytes were seeded on 96-well plates (Mattek, P96G-1.5-5-F). At 5 dpi, cell medium was replaced by DMEM without phenol red (Gibco, 31053028) and 0.5 mg/ml MTT was added. Cells were incubated at 37 °C and 5% CO2 for 4 h. Next, solubilization buffer (10% SDS in 0.01 M HCl) was added to the cells and used to solubilize formazan crystals. Absorbance was determined using a spectrophotometer (SPECTROstar Nano Microplate Reader, BMG LABTECH) at 570 nm and background absorbance at 690 nm was subtracted. Final absorbance signal is proportional to the number of metabolically active cells. Cells exposed to 1 mM hydrogen peroxide (H_2O_2) were taken as control, nonviable samples.

TUNEL assay in neonatal cardiomyocytes

Apoptotic damage was examined using a TUNEL assay kit following the recommendations of the provider (Roche, 11684795910). Briefly, neonatal cardiomyocytes were cultured on 24-well plates (Mattek, P24G-1.5-13-F). At 5 dpi, the cells were fixed with PFA for 10 min, permeabilized with 0.2% (v/v) Triton X-100 in 1% (w/v) BSA for 5 min. Treatment with 1 ng/ml DNase I before incubation with enzyme solution (TdT) served as positive control. As negative control, samples incubated with Label Solution (fluorescein-dUTP) alone were used. Fluorescent images were acquired using a Zeiss LSM700 confocal microscope with Plan-Apochromat 40x/1.3 Oil DIC M27 objective.

Beating analysis using MYOCYTER

Short videos of spontaneously beating single cardiomyocytes, lasting 14.26 s at 33.3 frames per second, were analyzed from 10 to 20 beating cardiomyocytes. MYOCYTER, an open-source macro for ImageJ, was used to determine contraction parameters (50). The macro measures contraction from the image differences between the resting state (reference image) and the subsequent frames. Peak times were estimated at 20% amplitude.

EdU assay

Nuclear EdU incorporation was used to evaluate cellular proliferation. EdU assays were performed with the Click-iT Plus EdU Alexa Fluor 647 Imaging Kit according to the manufacturer's protocol (Thermo Fisher Scientific). EdU was added to cardiomyocyte cultures 3 h before cell fixation according to the manufacturer's protocol.

Statistical analysis

In all figures, measurements are reported as mean ± SD or ± SEM. The number of independent experiments is specified in the figure legends. In the case of *in vitro* experiments, N represents the number of independent cardiomyocyte isolations, while technical replicates correspond to wells with independent infections. Statistical significance was evaluated using GraphPad Prism 10. Unpaired Student's two-sided *t* test were used to assess statistically significant differences between groups. Differences were considered statistically significant at $p < 0.05$. Nonsignificant differences are indicated as "ns".

Data availability

The data relating to this article are available in the article itself or in its Supplementary material online. The beating analysis data are available upon reasonable request to the corresponding authors.

Supporting information—This article contains supporting information (31, 32).

Acknowledgments—We acknowledge the personnel from CNIC animal facility and viral vectors. Light microscopy was conducted at the CNIC Microscopy & Dynamic Imaging Unit. We thank Verónica Labrador-Cantarero for her support with imaging analysis. We acknowledge the feedback from many colleagues at CNIC, especially Florian Weinberger, José Luis de la Pompa, Silvia Martin-Puig, and Hesham Sadek. We thank Mauro Giacca for insightful feedback. We thank Dieter Fürst for providing the T12 antibody. We thank all members of the Molecular Mechanics of the Cardiovascular System team for their support and input. We thank Alba Pobes-Lagartos for excellent technical assistance.

Author contributions—M. R. P. and J. A.-C. writing–review and editing; M. R. P. and J. A.-C. writing–original draft; M. R. P., M. A. L.-U., N. V., C. M.-L., W. P.-F., A. C. D., and F. M. E. investigation; M. R. P., M. A. L.-U., N. V., C. M.-L., W. P.-F., A. C. D., and F. M. E. formal analysis; M. R. P. and J. A.-C. data curation; M. R. P., M. A. L.-U., R. S.-R., E. H.-G., and J. A.-C. conceptualization; J. P.-P. M. I. S., R. G., and M. T. methodology.

Funding and additional information—J. A.-C. acknowledges funding from the European Research Council (ERC) under the European Union's Horizon 2020 research and innovation programme (grant agreement No. [101002927]). M. T. was funded by the ERC grant agreement N° 101142005. CNIC is supported by the Instituto de Salud Carlos III (ISCIII), the Ministerio de Ciencia, Innovación y Universidades (MCIU, MICIU/AEI/10.13039/501100011033) and the Pro CNIC Foundation, and is a Severo

Ochoa Center of Excellence (grant CEX2020-001041-S funded by MCIU). MALU is supported by grant FJC2021 047055-I from MCIU. J. A.-C. and R. G. acknowledge financial support from Comunidad de Madrid through grants Tec4Bio-CM (P2018/NMT-4443) and TecNanoBio-CM (TEC-2024/TEC-158). A. C. D. acknowledges funding from La Caixa Foundation [LCF/BQ/PI22/11910029]. J. P.-P. acknowledges a fellowship from "la Caixa" Foundation (ID 100010434), fellowship code LCF/BQ/DR22/11950017. R. S.-R. acknowledges funding from the European Molecular Biology Organization (EMBO, postdoctoral fellowship EMBO ALTF 417-2022). M. I. S. gratefully acknowledges financial support from the Wellcome Trust (225914/Z/22/Z).

Conflict of interest—The authors declare that they have no conflicts of interest with the contents of this article.

Abbreviations—The abbreviations used are: AAV, adeno-associated virus; CMV, cytomegalovirus; cTEV, cleaved TEV; DAPI, 4′,6-diamidino-2-phenylindole dihydrochloride; DEG, differentially expressed gene; dpi, days post infection; EdU, 5-ethynyl-2′-deoxyuridine; GO, gene ontology; MTT, 3-[4,5-dimethylthiazol-2-yl]-2,5- diphenyl tetrazolium bromide; PFA, paraformaldehyde; RT, room temperature; TEVp, tobacco etch virus protease; TTN, titin; TUNEL, terminal deoxynucleotidyl transferase dUTP nick end labeling.

References

1. Moran, A. E., Forouzanfar, M. H., Roth, G. A., Mensah, G. A., Ezzati, M., Murray, C. J. L., *et al.* (2014) Temporal trends in ischemic heart disease mortality in 21 world regions, 1980 to 2010. *Circulation* **129**, 1483–1492
2. Sadek, H., and Olson, E. N. (2020) Toward the goal of human heart regeneration. *Cell Stem Cell* **26**, 7–16
3. Pasumarthi, K. B. S., and Field, L. J. (2002) Cardiomyocyte cell cycle regulation. *Circ. Res.* **90**, 1044–1054
4. Porrello, E. R., Mahmoud, A. I., Simpson, E., Hill, J. A., Richardson, J. A., Olson, E. N., *et al.* (2011) Transient regenerative potential of the Neonatal Mouse heart. *Science* **331**, 1078–1080
5. Bergmann, O., Zdunek, S., Felker, A., Salehpour, M., Alkass, K., Bernard, S., *et al.* (2015) Dynamics of cell generation and turnover in the human heart. *Cell* **161**, 1566–1575
6. Hein, S., Arnon, E., Kostin, S., Schonburg, M., Elsasser, A., Polyakova, V., *et al.* (2003) Progression from compensated hypertrophy to failure in the pressure-overloaded human heart. *Circulation* **107**, 984–991
7. Uusimaa, P., Risteli, J., Niemela, M., Lumme, J., Ikaheimo, M., Jounela, A., *et al.* (1997) Collagen scar formation after acute myocardial infarction. *Circulation* **96**, 2565–2572
8. Poss, K. D., Wilson, L. G., and Keating, M. T. (2002) Heart regeneration in zebrafish. *Science* **298**, 2188–2190
9. Oberpriller, J. O., and Oberpriller, J. C. (1974) Response of the adult newt ventricle to injury. *J. Exp. Zool.* **187**, 249–259
10. Flink, I. (2002) Cell cycle reentry of ventricular and atrial cardiomyocytes and cells within the epicardium following amputation of the ventricular apex in the axolotl, Amblystoma mexicanum : confocal microscopic immunofluorescent image analysis of bromodeoxyuridine-labe. *Anat. Embryol.* **205**, 235–244
11. Canseco, D. C., Kimura, W., Garg, S., Mukherjee, S., Bhattacharya, S., Abdisalaam, S., *et al.* (2015) Human ventricular unloading induces cardiomyocyte proliferation. *J. Am. Coll. Cardiol.* **65**, 892–900
12. Senyo, S. E., Steinhauser, M. L., Pizzimenti, C. L., Yang, V. K., Cai, L., Wang, M., *et al.* (2013) Mammalian heart renewal by pre-existing cardiomyocytes. *Nature* **493**, 433–436
13. Bersell, K., Arab, S., Haring, B., and Kühn, B. (2009) Neuregulin1/ErbB4 signaling induces cardiomyocyte proliferation and repair of heart injury. *Cell* **138**, 257–270
14. Eulalio, A., Mano, M., Ferro, M. D., Zentilin, L., Sinagra, G., Zacchigna, S., *et al.* (2012) Functional screening identifies miRNAs inducing cardiac regeneration. *Nature* **492**, 376–381
15. Xin, M., Kim, Y., Sutherland, L. B., Murakami, M., Qi, X., McAnally, J., *et al.* (2013) Hippo pathway effector Yap promotes cardiac regeneration. *Proc. Natl. Acad. Sci. U. S. A.* **110**, 13839–13844
16. D'Uva, G., Aharonov, A., Lauriola, M., Kain, D., Yahalom-Ronen, Y., Carvalho, S., *et al.* (2015) ERBB2 triggers mammalian heart regeneration by promoting cardiomyocyte dedifferentiation and proliferation. *Nat. Cell Biol.* **17**, 627–638
17. Xin, M., Kim, Y., Sutherland, L. B., Qi, X., McAnally, J., Schwartz, R. J., *et al.* (2011) Regulation of insulin-like growth factor signaling by Yap governs cardiomyocyte proliferation and embryonic heart size. *Sci. Signal.* **4**, ra70
18. Engel, F. B., Hsieh, P. C. H., Lee, R. T., and Keating, M. T. (2006) FGF1/p38 MAP kinase inhibitor therapy induces cardiomyocyte mitosis, reduces scarring, and rescues function after myocardial infarction. *Proc. Natl. Acad. Sci. U. S. A.* **103**, 15546–15551
19. Gautel, M., and Djinović-Carugo, K. (2016) The sarcomeric cytoskeleton: from molecules to motion. *J. Exp. Biol.* **219**, 135–145
20. Ali, H., Braga, L., and Giacca, M. (2020) Cardiac regeneration and remodelling of the cardiomyocyte cytoarchitecture. *FEBS J.* **287**, 417–438
21. Fan, X., Hughes, B. G., Ali, M. A. M., Chan, B. Y. H., Launier, K., and Schulz, R. (2016) Matrix metalloproteinase-2 in oncostatin M-induced sarcomere degeneration in cardiomyocytes. *Am. J. Physiol. Circ. Physiol.* **311**, H183–H189
22. Xiao, F., Nguyen, N. U. N., Wang, P., Li, S., Hsu, C.-C., Thet, S., *et al.* (2024) Adducin regulates sarcomere disassembly during cardiomyocyte mitosis. *Circulation* **150**, 791–805
23. Pettinato, A. M., Yoo, D., VanOudenhove, J., Chen, Y.-S., Cohn, R., Ladha, F. A., *et al.* (2021) Sarcomere function activates a p53-dependent DNA damage response that promotes polyploidization and limits in vivo cell engraftment. *Cell Rep.* **35**, 109088
24. Yahalom-Ronen, Y., Rajchman, D., Sarig, R., Geiger, B., and Tzahor, E. (2015) Reduced matrix rigidity promotes neonatal cardiomyocyte dedifferentiation, proliferation and clonal expansion. *Elife* **4**, e07455
25. Linke, W. A., and Hamdani, N. (2014) Gigantic business. *Circ. Res.* **114**, 1052–1068
26. Granzier, H. L., and Labeit, S. (2025) Discovery of titin and its role in heart function and disease. *Circ. Res.* **136**, 135–157
27. Li, Y., Hessel, A. L., Unger, A., Ing, D., Recker, J., Koser, F., *et al.* (2020) Graded titin cleavage progressively reduces tension and uncovers the source of A-band stability in contracting muscle. *Elife* **9**, e64107
28. Silva-Rojas, R., Vicente, N., Gavilán-Herrera, M., Labarador-Cantero, V., Sicilia, J., Giménez-Sáez, O., *et al.* (2025) Mechanically knocking out titin reveals protein tension loss as a trigger of muscle disease. *Nat. Biomed. Eng.* **9**, 1758–1774
29. Rivas-Pardo, J. A., Li, Y., Mártonfalvi, Z., Tapia-Rojo, R., Unger, A., Fernández-Trasancos, Á., *et al.* (2020) A HaloTag-TEV genetic cassette for mechanical phenotyping of proteins from tissues. *Nat. Commun.* **11**, 2060
30. Loescher, C. M., Freundt, J. K., Unger, A., Hessel, A. L., Kühn, M., Koser, F., *et al.* (2023) Titin governs myocardial passive stiffness with major support from microtubules and actin and the extracellular matrix. *Nat. Cardiovasc. Res.* **2**, 991–1002
31. Sanchez, M. I., and Ting, A. Y. (2020) Directed evolution improves the catalytic efficiency of TEV protease. *Nat. Methods* **17**, 167–174
32. Fürst, D. O., Osborn, M., Nave, R., and Weber, K. (1988) The Organization of titin filaments in the half-sarcomere revealed by monoclonal antibodies in immunoelectron microscopy: a map of ten nonrepetitive epitopes starting at the Z line extends close to the M line. *J. Cell Biol.* **106**, 1563–1572
33. [preprint] López-Unzu, M. A., Pricolo, M. R., Silva-Rojas, R., Clemente-Manteca, A., Vicente, N., Velázquez-Carreras, D., *et al.* (2025) Titin cleavage is a driver of cardiomyocyte disengagement and reactive myocardial fibrosis. *bioRxiv*. https://doi.org/10.1101/2025.04.22.645683
34. Alvarez, R., Wang, B. J., Quijada, P. J., Avitabile, D., Ho, T., Shaitrit, M., *et al.* (2019) Cardiomyocyte cell cycle dynamics and proliferation

revealed through cardiac-specific transgenesis of fluorescent ubiquitinated cell cycle indicator (FUCCI). *J. Mol. Cell Cardiol.* **127**, 154–164
35. Li, B., Wei, Y., Guo, Y., Wang, Q., Gu, S., Ji, X., *et al.* (2024) Protocol to evaluate rat and mouse cardiomyocyte proliferation in vitro and in vivo. *STAR Protoc.* **5**, 103204
36. Monroe, T. O., Hill, M. C., Morikawa, Y., Leach, J. P., Heallen, T., Cao, S., *et al.* (2019) YAP partially reprograms chromatin accessibility to directly induce adult cardiogenesis *in vivo*. *Dev. Cell* **48**, 765–779.e7
37. Villa del Campo, C., Raiola, M., Sierra, R., MS, I., Peña-Peña, J., Esteban, I., *et al.* (2025) Myc overexpression improves recovery from myocardial infarction associated with cardiomyocyte hyperplasia in the mouse heart. *Commun. Biol.* **8**, 1069
38. Heusch, G. (2024) Myocardial ischemia/reperfusion: translational pathophysiology of ischemic heart disease. *Med* **5**, 10–31
39. Corrado, D., Link, M. S., and Calkins, H. (2017) Arrhythmogenic right ventricular cardiomyopathy. *N. Engl. J. Med.* **376**, 61–72
40. Fan, X., Hughes, B. G., Ali, M. A. M., Cho, W. J., Lopez, W., and Schulz, R. (2015) Dynamic alterations to α-Actinin accompanying sarcomere disassembly and reassembly during cardiomyocyte mitosis. *PLoS One* **10**, e0129176
41. Ahuja, P., Perriard, E., Perriard, J.-C., and Ehler, E. (2004) Sequential myofibrillar breakdown accompanies mitotic division of mammalian cardiomyocytes. *J. Cell Sci.* **117**, 3295–3306
42. Kubin, T., Pöling, J., Kostin, S., Gajawada, P., Hein, S., Rees, W., *et al.* (2011) Is a major mediator of cardiomyocyte dedifferentiation and remodeling. *Cell Stem Cell* **9**, 420–432
43. Lahmers, S., Wu, Y., Call, D. R., Labeit, S., and Granzier, H. (2004) Developmental control of Titin Isoform expression and passive stiffness in fetal and neonatal myocardium. *Circ. Res.* **94**, 505–513
44. Nielsen, M. S., van Opbergen, C. J. M., van Veen, T. A. B., and Delmar, M. (2023) The intercalated disc: a unique organelle for electromechanical synchrony in cardiomyocytes. *Physiol. Rev.* **103**, 2271–2319
45. Tabebordbar, M., Lagerborg, K. A., Stanton, A., King, E. M., Ye, S., Tellez, L., *et al.* (2021) Directed evolution of a family of AAV capsid variants enabling potent muscle-directed gene delivery across species. *Cell* **184**, 4919–4938.e22
46. Schindelin, J., Arganda-Carreras, I., Frise, E., Kaynig, V., Longair, M., Pietzsch, T., *et al.* (2012) Fiji: an open-source platform for biological-image analysis. *Nat. Methods* **9**, 676–682
47. Boudaoud, A., Burian, A., Borowska-Wykręt, D., Uyttewaal, M., Wrzalik, R., Kwiatkowska, D., *et al.* (2014) FibrilTool, an ImageJ plug-in to quantify fibrillar structures in raw microscopy images. *Nat. Protoc.* **9**, 457–463
48. Stringer, C., Wang, T., Michaelos, M., and Pachitariu, M. (2021) Cellpose: a generalist algorithm for cellular segmentation. *Nat. Methods* **18**, 100–106
49. [preprint] Schmidt, U., Weigert, M., Broaddus, C., and Myers, G. (2018) Cell detection with star-convex polygons. *arXiv*. https://doi.org/10.48550/arXiv.1806.03535
50. Grune, T., Ott, C., Häseli, S., Höhn, A., and Jung, T. (2019) The "MYOCYTER" – convert cellular and cardiac contractions into numbers with ImageJ. *Sci. Rep.* **9**, 15112